Journal of Power Sources 257 (2014) 120–125

Contents lists available at ScienceDirect

Journal of Power Sources

journal homepage: www.elsevier.com/locate/jpowsour

Two-phase separation in a lithiated spinel $Li_4Ti_5O_{12}$ crystal as confirmed by electron energy-loss spectroscopy

Mitsunori Kitta*, Tomoki Akita, Shingo Tanaka, Masanori Kohyama

Research Institute for Ubiquitous Energy Devices, National Institute of Advanced Industrial Science and Technology (AIST), 1-8-31 Midorigaoka, Ikeda, Osaka 563-8577, Japan

HIGHLIGHTS

- Separation of $Li_4Ti_5O_{12}$ and $Li_7Ti_5O_{12}$ phases in a LTO crystal sample was identified by STEM–EELS.
- Single crystalline LTO specimen for TEM analysis was prepared by Li-VIG method.
- Two-phase boundary is formed parallel to the <011> direction by the preferential Li-ion diffusion.

GRAPHICAL ABSTRACT

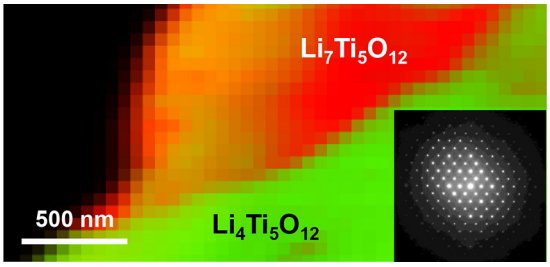

ARTICLE INFO

Article history:
Received 15 October 2013
Received in revised form
10 January 2014
Accepted 14 January 2014
Available online 5 February 2014

Keywords:
Li-ion battery
$Li_4Ti_5O_{12}$
Single-crystalline study
Two-phase separation
Electron energy-loss spectroscopy

ABSTRACT

The coexistence state of two phases ($Li_4Ti_5O_{12}$ and lithiated $Li_7Ti_5O_{12}$) in spinel lithium titanium oxide (LTO; $Li_4Ti_5O_{12}$) is examined using scanning transmission electron microscopy with electron energy-loss spectroscopy (STEM–EELS). A single crystalline LTO specimen is prepared from a TiO_2 wafer and is then partially lithiated. STEM–EELS spectrum imaging of the lithiated specimen reveals that the two phases exist separately inside the specimen with phase boundaries, and no apparent misfit strains or misorientations are detected. The phase interface appears to be preferentially formed parallel to the (100) plane owing to preferential Li diffusion along the <011> and equivalent directions in the LTO crystal. The observed two-phase morphology can be explained by the fact that relative to solid solutions, the $Li_7Ti_5O_{12}$ phase can accommodate inserted Li atoms with negligible lattice distortions or volume changes in the common Ti–O bond framework.

1. Introduction

Spinel lithium titanium oxide [1–4] (LTO; $Li_4Ti_5O_{12}$, space group *Fd-3m*) has attracted attention as one of the most promising candidates for anode materials of large-scale lithium-ion batteries. This is because of the excellent charge–discharge performance and the long life of spinel LTO [5,6]. Spinel LTO shows a remarkable constant charge–discharge potential of around 1.55 vs. Li^+/Li in the capacity–voltage profile during the charge–discharge cycle, corresponding to a two-phase transition process between $Li_4Ti_5O_{12}$ spinel and $Li_7Ti_5O_{12}$ ordered rock salt phases, according to the following proposed general equation [2,4,7]:

$$(Li_3)^{8a}(LiTi_5)^{16d}(O_{12})^{32e} + 3Li^+ + 3\,e^- \rightarrow (Li_6)^{16c}(LiTi_5)^{16d}(O_{12})^{32e} \quad (1)$$

where the superscripts stand for the number of equivalent sites with Wyckoff symbols for the space group *Fd-3m*. In this electrochemical Li-insertion process, additional lithium ions are inserted into octahedral 16c sites; simultaneously, all the lithium ions at tetrahedral 8a sites are then shifted to 16c sites [4]. The rigid spinel

* Corresponding author. Tel.: +81 072 751 8703; fax: +81 072 751 9714.
E-mail address: m-kitta@aist.go.jp (M. Kitta).

0378-7753/$ – see front matter © 2014 Elsevier B.V. All rights reserved.
http://dx.doi.org/10.1016/j.jpowsour.2014.01.069

framework $(LiTi_5)^{16d}(O_{12})^{32e}$ provides a three-dimensional network of channels for facile lithium diffusion [7] and exhibits an extremely small change in the unit-cell volume from $Li_4Ti_5O_{12}$ ($a = 0.83595$ nm [7,8]) to $Li_7Ti_5O_{12}$ ($a = 0.83538$ nm [7]), leading to the zero strain property, [4,8,9] and excellent stability for high-rate charge–discharge performance [6,10].

Since the two-phase mechanism results in excellent charge–discharge performance for LTO, it is crucial to investigate in detail the two-phase coexistence state in partially lithiated LTO. For this purpose, we previously investigated the two-phase distribution in a commercial $Li_4Ti_5O_{12}$ secondary particle consisting of primary particles by scanning transmission electron microscopy with electron energy-loss spectroscopy (STEM–EELS). We observed the presence of both considerably or fully lithiated primary particles and pristine or slightly lithiated primary particles in a half Lithiated secondary particle [11]. This result suggests that the Li insertion extends from a primary particle to a neighboring primary particle in a secondary particle, and the rate-determining process for the Li-insertion reaction occurs at the boundaries between primary particles. However, the detailed process of Li insertion in each primary crystalline particle itself is yet unclear, and the question of whether the two phases exist separately or hybridized as a solid solution, $Li_{4+x}Ti_5O_{12}$ ($0 < x < 3$), during the process of lithiation of one primary particle still remains to be answered [12–14]. Therefore, characterization of the two-phase coexistence in single-crystalline LTO is quite important to understand the two-phase mechanism responsible for a stable charge–discharge potential and high-rate charge–discharge performance.

In this study, we investigate in detail the distribution of the two phases, namely, $Li_4Ti_5O_{12}$ and $Li_7Ti_5O_{12}$, in a single-crystalline LTO sample with partial lithiation by using TEM and STEM–EELS observations.

2. Experimental

2.1. Preparation of a single-crystalline $Li_4Ti_5O_{12}$ specimen for TEM analysis

In this study, we observe single-crystalline LTO samples by using TEM. First, we prepare a single-crystalline LTO specimen for TEM observations from a rutile TiO_2 wafer by the procedure shown in Fig. 1(a). A commercial TiO_2 wafer (Shinkosha, Co., Ltd.) is polished as a thin specimen by using an Ar^+ ion polishing system (PIPS, Gatan, Inc.). The polished TiO_2 wafer is then calcined with $LiOH{\cdot}H_2O$ in air at 1127 K for 18 h in a 99% alumina crucible. In the calcination process, thin edges of the polished TiO_2 wafer react with the vaporized Li source and are transformed into $Li_4Ti_5O_{12}$ single crystals. In other words, Li vapor induces single-crystalline $Li_4Ti_5O_{12}$ growth at the edges, and thus, we name this method as Li-vapor induction growth (Li-VIG). In this process, the orientation of LTO crystal growth is controlled by the TiO_2 wafer orientation. Similar to our previous study [15], in this study too we confirm the preferential (111)-oriented growth of $Li_4Ti_5O_{12}$ prepared from the TiO_2 (111) wafer, owing to their similarity in the in-plane atomic periodicity. We also observe (100)- and (110)-oriented preferential growth of LTO prepared from TiO_2 (110) and (001) wafers, respectively, as shown in Fig. 1(b).

The crystallinity of the prepared $Li_4Ti_5O_{12}$ specimen is examined by electron diffraction and high-resolution (HR)-TEM analysis. The TEM apparatus (JEM-3000F, JEOL) is used at 200 kV in the bright field (BF)-TEM mode. The data are recorded by GIF (Gatan, Inc.)

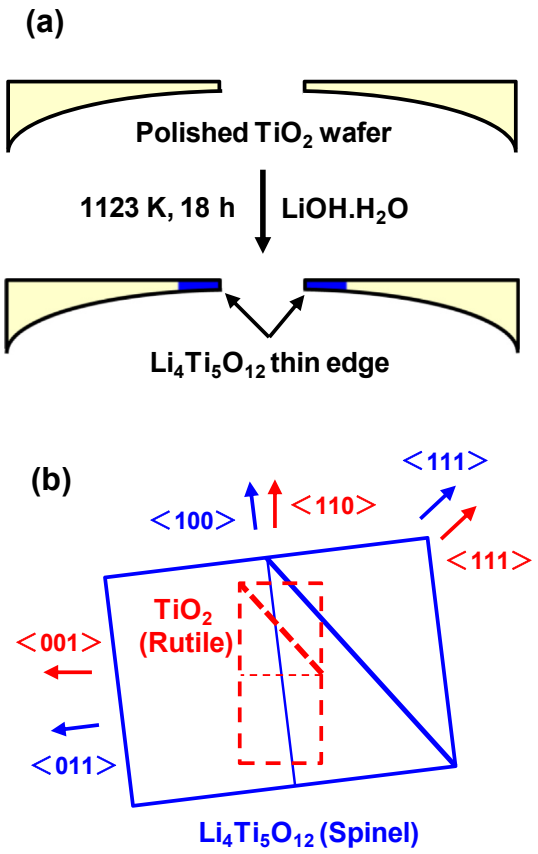

Fig. 1. (a) Schematic for the preparation of a single-crystal $Li_4Ti_5O_{12}$ specimen. $Li_4Ti_5O_{12}$ single crystals are formed at damaged thin edges of a polished TiO_2 wafer by calcination with $LiOH{\cdot}H_2O$, which is called Li-vapor induction crystal growth (Li-VIG). (b) Relation between the growth orientations of a spinel $Li_4Ti_5O_{12}$ crystal (blue) and a rutile TiO_2 wafer (red). Both crystals were aligned along the <1–10> axis as the normal to the figure. A spinel $Li_4Ti_5O_{12}$ crystal grew in the <111> direction for the rutile (111) surface plane. (For interpretation of the references to color in this figure legend, the reader is referred to the web version of this article.)

2.2. Preparation of two-phase coexistence state in a single-crystalline $Li_4Ti_5O_{12}$ specimen

To prepare the two-phase coexistence state, we perform partial Li-metal deposition on single-crystalline $Li_4Ti_5O_{12}$ by using the vacuum vapor deposition process. A commercial evaporation source (lithium metal dispenser, SAES Getters) is electrically heated under 8.0 A with 3.0 V in vacuum-coating equipment (JEE-420, JEOL). After Li-metal deposition, the LTO thin edge is turned black, indicating the partial occurrence of the following redox reaction:

$$3Li + Li_4Ti_5O_{12} \rightarrow Li_7Ti_5O_{12} \quad (2)$$

Because the deposited Li metal acts as a reducing agent owing to its low redox potential, the portion of the $Li_4Ti_5O_{12}$ crystal in contact with Li metal should be transformed to a $Li_7Ti_5O_{12}$ phase. The deposited sample is then placed in a dry-air-filled box for 5 days to complete the lithiation reaction and two-phase relaxation [12,13].

The two-phase coexistence state is examined via STEM–EELS by using analytical TEM (TITAN^{3TM} G2, FEI) in the 200-kV STEM mode with a Wien-filtered monochromator. The two phases, namely, $Li_4Ti_5O_{12}$ and $Li_7Ti_5O_{12}$, can be identified by the features of Ti-$L_{3,2}$ edge and O–K edge regions in the energy-loss near-edge structure (ELNES), as examined in Ref. [11]. The EELS data recording is simultaneously performed in Ti-$L_{3,2}$ edge and O–K edge regions at

0.05 eV/channel dispersion and with a 0.25 eV FWHM energy resolution for the zero-loss peak. Spectrum imaging (SI) data are acquired in 50 nm pixel steps with a 50 × 50 pixel resolution at a read out time of 0.05 s. The acquired SI image is reconstructed with a different phase mapping via the multiple linear least square (MLLS) fitting using the shape of the Ti-$L_{2,3}$ edge [11].

3. Results and discussion

3.1. Prepared single-crystalline LTO specimen

Fig. 2(a)–(c) show the low-magnification BF-TEM images of the $Li_4Ti_5O_{12}$ specimens prepared from TiO_2 (110), (001), and (111) wafers. All the samples appear to be LTO single crystals at least in the observed area, and reveal typical shaped edges of thick regions as typical facets of each crystal-growth orientation, reflecting stable surfaces during the crystal growth. There are no contaminations, cracks, or deficiency contrast at least in a ~5 × 5 μm^2 area in Fig. 2(a)–(c). Fig. 2(d)–(f) show the electron diffraction patterns acquired from the area shown in Fig. 2(a)–(c). All the diffraction spots in Fig. 2(d)–(f) show the spinel feature, but do not show other extra spots. These results indicate that the three specimens are $Li_4Ti_5O_{12}$ single crystals without any residual TiO_2 phases or other contamination phases such as β-Li_2TiO_3, at least in a ~5 × 5 μm^2 area. Further, the diffraction patterns indicate that the specimens prepared from TiO_2 (110), (001), and (111) wafers have [100], [110], and [111] orientations along the incident direction, respectively, as shown in Fig. 1(b).

3.2. Characterization of a partially lithiated LTO crystalline specimen

The two-phase coexistence in a single crystalline specimen after the partial Li-metal deposition (explained in Sec. 2.2) is investigated by ADF–STEM and STEM–EELS, as shown in Fig. 3. The typical crystal facets of a $Li_4Ti_5O_{12}$ (110) specimen are indexed in the low-magnification ADF–STEM image of Fig. 3(a), where (100) and (111) edges can be assigned to regular facet angles, similar to the case of the LTO specimen shown in Fig. 2(b). From the ADF–STEM image, we cannot find any distinction or boundaries between the two phases, i.e., $Li_4Ti_5O_{12}$ and $Li_7Ti_5O_{12}$, and the whole specimen appears to be a single crystal. The STEM–EELS spectrum image in Fig. 3(b), however, clearly shows the distribution of the two phases, i.e., $Li_4Ti_5O_{12}$ and $Li_7Ti_5O_{12}$. The spectrum image data, acquired from the yellow square area in Fig. 3(a), are reconstructed for the difference between the Ti-*L* edge feature of the two phases via MLLS fitting [11]. The Ti-$L_{3,\ 2}$ and O–*K* edge ELNES spectra extracted from points 1 and 2 in Fig. 3(b) are shown in Fig. 3(c). Both the Ti-$L_{3,\ 2}$ and O–*K* edge features of these two spectra are clearly different from each other. The spectrum extracted from point 1 (Sp. 1) has four main peaks in the Ti-*L* edge region, representing t_{2g}–e_g splitting of each L_2 and L_3 peak as Ti^{4+} in $Li_4Ti_5O_{12}$. On the other hand, two broad peaks are observed in the spectrum from point 2 (Sp. 2), similar to the case of bulk $Li_7Ti_5O_{12}$ reported previously [11]. The spectra in the O–*K* edge region of Sp. 1 and Sp. 2 also reveal the features of $Li_4Ti_5O_{12}$ and $Li_7Ti_5O_{12}$, respectively [11]. From these results, we can ascertain that the green region (including Sp. 1) and red region (including Sp. 2) correspond to $Li_4Ti_5O_{12}$ and $Li_7Ti_5O_{12}$, respectively.

The distribution morphology of these two phase regions in the crystal sample appears to depend on the crystal orientation. The crystal orientation in Fig. 3(b) can be defined from the facet assignment in Fig. 3(a). The two-phase interface appears to exist parallel to the (100) LTO crystal plane and along the <011> direction of LTO in Fig. 3(b). As explained above, the Lithiated phase is formed by Li insertion at the 16c sites and simultaneous shifts of pre-existing Li at the 8a sites to the 16c sites, with the Ti(Li)–O bonding framework remaining common between the 16d and 32e sites. Thus, the two-phase interface is naturally formed during the lithiated phase generation via Li diffusion, and the morphology of this interface can be explained by the diffusion ability of Li ions in the LTO bulk crystal. The Li-ion diffusion in the <100>direction appears to be inferior to that in the <011>direction in the bulk LTO, owing to the non-existence of a tetrahedral 8a site channel pathway to facilitate Li-ion transfer [12], [16–19] in this direction (as shown in Fig. 4). Thus, the growth of the Lithiated phase is

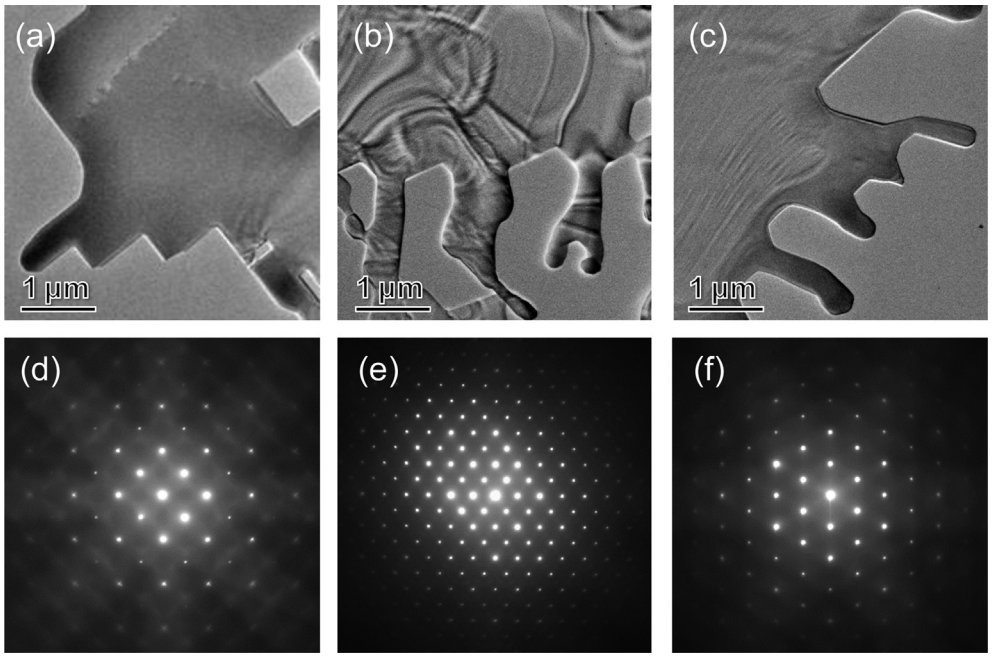

Fig. 2. HR-TEM micrograph of spinel $Li_4Ti_5O_{12}$ specimens prepared from (a) rutile TiO_2 (110), (b) (001), and (c) (111) wafers. (d)–(f) Electron diffraction patterns acquired from areas of (a)–(c).

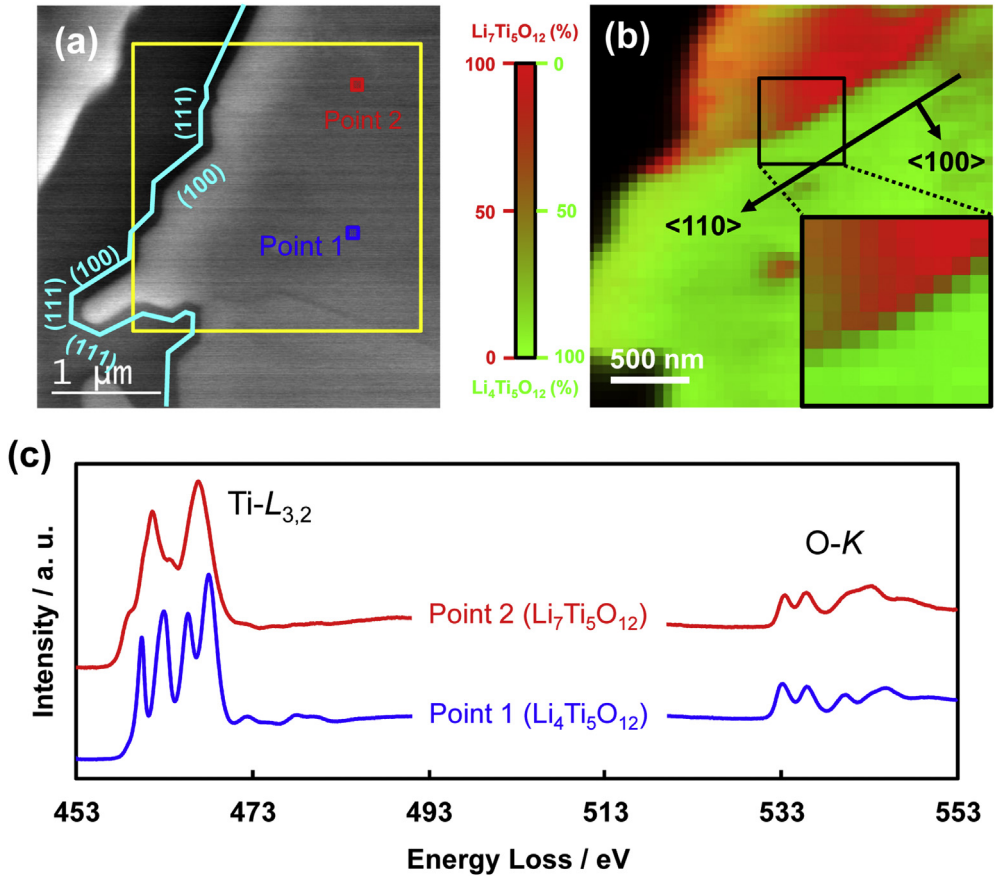

Fig. 3. (a) ADF–STEM image of a partially lithiated single-crystalline $Li_4Ti_5O_{12}$ (110) specimen. (b) STEM–EELS spectrum image, acquired from the yellow square region in (a). The image was reconstructed by the MLLS fitting of the Ti-$L_{3,2}$ ELNES feature shown in (c). Spectra extracted from points 1 and 2 in (a) are shown in (c). (For interpretation of the references to color in this figure legend, the reader is referred to the web version of this article.)

suppressed in the <100>direction in contrast to the <011> and equivalent directions normal to the <100>axis, resulting in the interface being parallel to the <011>direction.

The inset of Fig. 3(b) (the enlarged image of square area) shows mixtures of the ELNES features of the two phases near their interface. This region can be interpreted at least as follow, first is a solid solution or some atomistic mixture, and the second is a simple overlap of two separated phases along the electron-beam direction. In order to examine these two possibilities, we apply the MLLS analysis to the spectra extracted near the interface, as shown in Fig. 5. All the extracted spectra are normalized by the maximum intensity of the Ti-*L* edge peaks, and are displayed in the order of the arrow in the inset of Fig. 5. The spectra of the end members, i.e., $Li_4Ti_5O_{12}$ and $Li_7Ti_5O_{12}$, are shown as No. 1 and No. 10, respectively. These two spectra show remarkable differences in the Ti-$L_{3,2}$ edge and O–*K* edge regions, similar to the spectra shown in Fig. 3(c), while the spectra of Nos. 2–9 show mixed features of these two spectra.

Here, we examine whether each spectrum of Nos. 2–9 can be expressed by a simple linear combination of No. 1 and No. 10 spectra by using a trial function $F_{(E)}$ as follows:

$$F_{(E)} = a f_{1(E)} + (1 - a) f_{10(E)} \tag{3}$$

where $f_{1(E)}$ and $f_{10(E)}$ denote the spectra of No. 1 and No. 10, respectively, as the base functions in this analysis, and a denotes the coefficient of linear combination. The coefficient a is fitted so as to minimize the residual sum of squares (RSS)

$$\mathrm{RSS} = \sum_i \left(F_{(E_i)} - f_{n(E_i)}\right)^2 \tag{4}$$

in some range of the energy E for the spectrum $f_{n(E)}$. Fig. 6(a) shows an example of fitting for the spectrum of No. 3, where we use the Ti-*L* energy region (455–475 eV) and RSS reaches the minimum value (0.058) with $a = 0.79$. In Fig. 6(a), the agreement between the fitted function $F_{3(E)}$ and the object function $f_{3(E)}$ is satisfactory, indicating that the spectrum of No. 3 can be expressed only by $f_{1(E)}$ and $f_{10(E)}$. Thus, we can say that the position of No. 3 consists of a simple overlap of the two separate phases along the electron beam direction. Note that the presence of a substantial ratio of solid-solution-like regions should lead to spectrum components that cannot be simply expressed by linear mixing.

Fig. 6(b) summarizes the results of the present analysis for No. 2 to No. 9. The results of fitting are essentially similar, as provided in Supporting information. The RSS value for each spectrum is less than 0.16, and thus, it can be said that all the spectra from No. 2 to No. 9 can be reproduced linearly by the two components of No. 1 and No. 10. Therefore, we conclude that the region of the ELNES spectra with mixed features in Fig. 3(b) indicates a simple overlap of two separate phases along the electron beam direction. The gradual change in the values of a in Fig. 6(b) appears to indicate that a flat interface is introduced between the two phases in some orientation inclined to the electron-beam direction. At present, we cannot comment on the detailed orientations or configurations of such inclined interfaces as well as those of the sharp interface in Fig. 3(b), which should be examined in the near future. However,

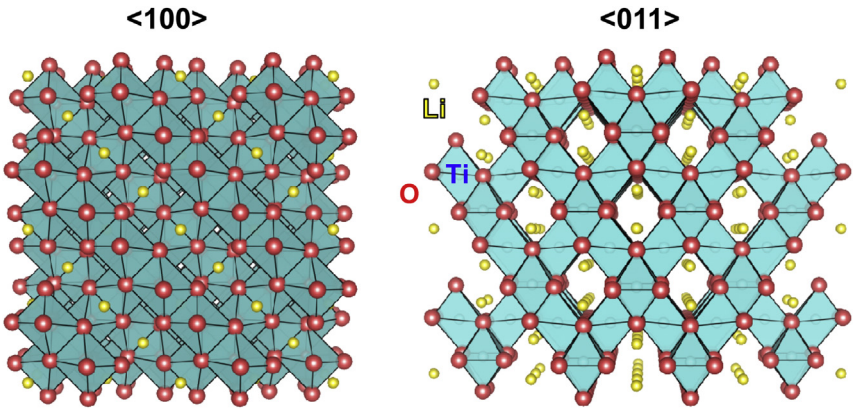

Fig. 4. Crystal structure of $Li_4Ti_5O_{12}$ as viewed from <100> and <011> directions.

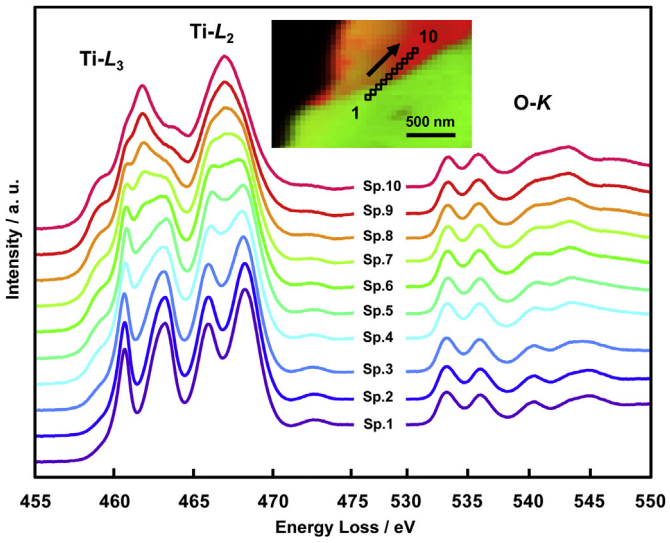

Fig. 5. Ti-*L* and O–K spectra extracted from points 1 to 10 (along the phase interface) in the inset figure.

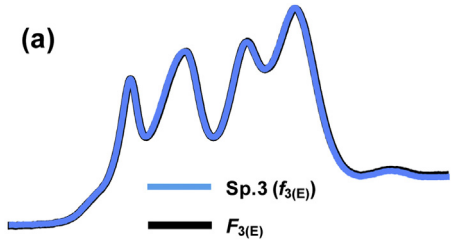

(b)

Sp.	2	3	4	5	6	7	8	9
a(%)	97	79	54	48	39	29	20	7.4
RSS ($\times 10^3$)	1.2	58	14	162	9.3	3.4	3.2	7.3

Fig. 6. (a) Comparison between the Ti-*L* edge region spectrum of point 3 (Fig. 5) and fitted spectrum $F_{3(E)}$ obtained by the linear combination of the spectra from Sp. 1 ($Li_4Ti_5O_{12}$) and Sp. 2 ($Li_7Ti_5O_{12}$). (b) Summary of similar fitting for all extracted spectra in Fig. 4.

we can say that we confirmed two-phase separation in this specimen with abrupt phase boundaries identified at least in the grid scale (50 nm steps in Fig. 3(b)).

3.3. Two-phase coexistence in a partially lithiated LTO crystalline specimen

The present analysis suggests that Lithiated LTO, namely, $Li_7Ti_5O_{12}$, is formed in an LTO ($Li_4Ti_5O_{12}$) single crystal, with the basic spinel framework remaining intact, and that the two phases exist separately with apparent phase interfaces. Moreover, the present observations indicate no apparent strains, misorientations, or defects at such phase interfaces. The interface appears to have preferential orientations, while detailed atomic-scale morphologies should be examined in the near future. The present results are consistent with the two-phase coexistence model, as per electrochemical considerations [4,7].

However, the present results are in contrast to those suggested by the solid-solution model [12,13]. From XRD results, Wagemeker and co-workers proposed that the separated two-phase state is stable only under 100 K, and that at room temperature, it becomes a uniform solid-solution phase ($Li_{4+x}Ti_5O_{12}$) as an equilibrium state [13]. Later, on the basis of NMR results, they proposed that the solid solution should consist of nanosized domains with the 8a-site Li ($Li_4Ti_5O_{12}$) and 16c-site Li ($Li_7Ti_5O_{12}$) structures [12]. Note that such diffraction or spectroscopic results can only lead to candidates with real microstructures, and cannot necessarily be used as direct evidence for real microstructures. Only real-space observations can provide direct evidence of real microstructures.

We think that the $Li_7Ti_5O_{12}$ phase should be naturally formed by Li insertion in LTO. Here, we consider how a large amount of Li atoms can be accommodated into LTO without a large increase in energy. Initially, a low density of Li atoms should be inserted at 16c sites as the largest interstitial space in spinel LTO, while relatively short distances between the inserted Li atoms and surrounding Li atoms at the 8a sites ($\sim$0.18 nm, which is almost half of the Li–Li or Li–Ti distance (0.3 nm) in LTO and $Li_7Ti_5O_{12}$ phases) should induce a local lattice distortion or lattice volume expansion in the spinel Ti–O bond framework. This should prevent further adsorption of Li. On the other hand, as indicated in Refs. [9,18,20], if the shift of the neighboring Li atoms from the 8a sites to the 16c sites occurs simultaneously with the reduction of nearby Ti ions from Ti^{4+} to Ti^{3+} by the valence electrons of inserted Li atoms, the Li atoms are stably accommodated with negligible lattice distortions or lattice volume changes. This only corresponds to the local formation of the Li–LTO ($Li_7Ti_5O_{12}$) phase with a closed-packed rock-salt structure having proper interatomic distances. Note that both the LTO and

Li–LTO phases have a common Ti(Li)–O bonding framework as $(LiTi_5)^{16d}(O_{12})^{32e}$ and almost an equal lattice volume, in spite of much higher Li density in the latter phase.

As a model of a solid-solution structure, an LTO crystal with high density of interstitial Li atoms at 16c sites without any shifts of surrounding Li atoms at 8a sites should contain remarkable volume changes, lattice distortions, and energy increases, as compared to the local formation of Li–LTO phases in LTO, which should occur smoothly owing to negligible strains or volume changes at the Li–LTO/LTO interface.

It is possible to imagine the structure for a mixture of nanosized domains [12] of the two phases without substantial distortions or volume changes, while a Li–LTO region with high density of Li ions is always accompanied by Ti reduction nearby, indicating that too small sizes of domains are unstable. Of course, a high temperature should possibly decrease the free energies of disordered phases to be lower than the separated two-phase state. However, our present results for partially lithiated LTO clearly show that the two-phase separation state is a thermodynamically equilibrium state at room temperature, as compared to a uniform solid solution or nanodomain structure [12,13].

The microstructure of a partially lithiated LTO crystal may depend on the lithiation process or particle size. In experiments involving charge–discharge cycles of actual LTO electrodes, the two-phase behavior of LTO particles is investigated for the kinetic process of a propagating redox reaction front dominated by electric and mass transport. For the two-phase morphology of LTO electrode particles during the actual charge–discharge processes, various models such as the core–shell structure model [6,10,21,22] and island structure model [23] have been proposed. Our previous STEM–EELS observation of secondary particles [11] indicated that the transport across the interface between primary particles is the rate-determining process. With regard to the two-phase behavior inside each primary particle, our present results suggest that the two-phase interface propagates with the reaction front inside the particle, which is indeed consistent with the above-mentioned models for actual electrode particles.

Of course, the present observation of the phase distribution in Fig. 3(b) does not provide details of the phase-interface structure at the nano- or sub-nanoscale. Thus, at present, we cannot comment on the detailed morphology of the phase interface and on how steeply or gradually the crystal structure, Li concentration, or Li-site occupancy changes at the interface. Thus, we will perform atomic-scale observations of the phase boundaries, attempts for which have recently begun [24].

4. Conclusions

The two-phase coexistence state in a lithiated $Li_4Ti_5O_{12}$ single crystal was revealed by STEM–EELS observations. A single crystalline $Li_4Ti_5O_{12}$ specimen was prepared from a TiO_2 wafer by the Li-VIG method, and the partial lithiation of the LTO specimen was attained by Li-metal vacuum deposition. The features of Ti-$L_{3,2}$ edge and O–K edge ELNES suggested that both the $Li_4Ti_5O_{12}$ and $Li_7Ti_5O_{12}$ phases exist separately within a single crystal. Spectrum imaging of the reconstructed data for the Ti-$L_{3,2}$ edge region revealed that the interface between the two phases was formed parallel to the (100) plane in the LTO crystal, which can be explained by the preferential Li diffusion in the <011> and equivalent directions normal to the <100>axis in the LTO crystal. Regions showing mixed features of ELNES were observed; such regions can be attributed to a simple overlap of the two phases separated by an inclined phase interface, instead of some solid solution phase. These results suggested that the two phases exist separately in an original LTO single crystal during lithiation. The present two-phase coexistence morphology can be explained by the fact that the $Li_7Ti_5O_{12}$ phase can accommodate inserted Li atoms with negligible lattice distortions or volume changes in the common Ti–O bonding framework.

Acknowledgment

The authors thank C. Fukada and M. Makino for their beneficial assistance in sample preparation. This work was supported by the Japan Society for the Promotion of Science (JSPS Grant-in-Aid for Scientific Research (B) 22360279).

Appendix A. Supplementary data

Supplementary data related to this article can be found at http://dx.doi.org/10.1016/j.jpowsour.2014.01.069.

References

[1] A. Deschanvres, B. Raveau, Z. Sekkal, Mater. Res. Bull. 6 (1971) 699–704.
[2] K.M. Colbow, J.R. Dahn, R.R. Haering, J. Power Sources 26 (1989) 397–402.
[3] E. Ferg, R.J. Gummov, A. de Kock, M.M. Thackeray, J. Electrochem. Soc. 141 (1994) L147–L150.
[4] T. Ohzuku, A. Ueda, N. Yamamoto, J. Electrochem. Soc. 142 (1995) 1431–1435.
[5] N. Takami, H. Inagaki, T. Morita, Toshiba Rev. 61 (2006) 6–10.
[6] N. Takami, H. Inagaki, T. Kishi, Y. Harada, Y. Fujita, H. Hoshina, J. Electrochem. Soc. 156 (2009) A128–A132.
[7] S. Scharner, W. Weppner, P. Schmid-Beurmann, J. Electrochem. Soc. 146 (1999) 857–861.
[8] K. Kataoka, Y. Takahashi, N. Kijima, H. Hayakawa, J. Akimoto, K. Ohshima, Solid State Ionics 180 (2009) 631–635.
[9] K. Ariyoshi, R. Yamato, T. Ohzuku, Electrochim. Acta 51 (2005) 1125–1129.
[10] N. Takami, K. Hoshina, H. Inagaki, J. Electrochem. Soc. 158 (2011) A725–A730.
[11] M. Kitta, T. Akita, S. Tanaka, M. Kohyama, J. Power Sources 237 (2013) 26–32.
[12] M. Wagemaker, E.R.H. van Eck, A.P.M. Kentgens, F.M. Mulder, J. Phys. Chem. B 113 (2009) 224–230.
[13] M. Wagemaker, D.R. Simon, E.M. Kelder, J. Schoonman, C. Ringpfeil, U. Haake, D. Lützenkirchen-Hecht, R. Frahm, F.M. Mulder, Adv. Mater. 18 (2006) 3169–3173.
[14] F. Ronci, P. Reale, B. Scrosati, S. Panero, V.R. Albertini, P. Perfetti, M. di Michiel, J.M. Merino, J. Phys. Chem. B 106 (2002) 3082–3086.
[15] M. Kitta, T. Akita, Y. Maeda, M. Kohyama, Appl. Surf. Sci. 258 (2012) 3147–3151.
[16] M. Wilkening, R. Amade, W. Iwaniak, P. Heitjans, Phys. Chem. Chem. Phys. 9 (2007) 1239–1246.
[17] V.W.J. Verhoeven, I.M. de Schepper, G. Nachtegaal, A.P.M. Kentgens, E.M. Kelder, J. Schoonman, F.M. Mulder, Phys. Rev. Lett. 86 (2001) 4315–4317.
[18] M. Anicete-Santos, L. Gracia, A. Beltrán, J. Andrés, J.A. Varela, E. Longo, Phys. Rev. B 77 (2008) 085112.
[19] I.A. Leonidov, O.N. Leonidova, L.A. Perelyaeva, R.F. Samigullina, S.A. Kovyazina, M.V. Patrakeev, Phys. Solid State 45 (2003) 2079–2085.
[20] K. Kataoka, Y. Takahashi, N. Kijima, H. Hayakawa, J. Akimoto, K. Ohshima, Solid State Ionics 180 (2009) 631–635.
[21] W. Lu, I. Belharouak, J. Liu, K. Amine, J. Electrochem. Soc. 154 (2007) A114–A118.
[22] J. Ma, C. Wang, S. Wroblewski, J. Power Sources 164 (2007) 849–856.
[23] D. Li, P. He, H. Li, H. Zhou, Phys. Chem. Chem. Phys. 14 (2012) 9086–9091.
[24] X. Lu, L. Zhao, X.Q. He, R.J. Xiao, L. Gu, Y.-S. Hu, H. Li, Z.-X. Wang, X.-F. Duan, L.-Q. Chen, J. Maier, Y. Ikuhara, Adv. Mater. 24 (2012) 3233–3238.